Journal of Inorganic Biochemistry 107 (2012) 119–128

Contents lists available at SciVerse ScienceDirect

Journal of Inorganic Biochemistry

journal homepage: www.elsevier.com/locate/jinorgbio

An *in vitro* comparative assessment with a series of new triphenyltin(IV) 2-/4-[(*E*)-2-(aryl)-1-diazenyl]benzoates endowed with anticancer activities: Structural modifications, analysis of efficacy and cytotoxicity involving human tumor cell lines

Tushar S. Basu Baul [a,*], Anup Paul [a], Lorenzo Pellerito [b], Michelangelo Scopelliti [b], Andrew Duthie [c], Dick de Vos [d], Rajeshwar P. Verma [e,1], Ulli Englert [f]

[a] Department of Chemistry, North-Eastern Hill University, NEHU Permanent Campus, Umshing, Shillong 793 022, India
[b] Dipartimento di Chimica "Stanislao Cannizzaro", Università degli Studi di Palermo, Viale delle Scienze, Parco D'Orleans II, Edificio 17, 90128 Palermo, Italy
[c] School of Life & Environmental Science, Deakin University, Geelong Victoria 3217, Australia
[d] Pharmachemie BV, PO Box 552, 2003 RN Haarlem, The Netherlands
[e] Department of Chemistry, Pomona College, 645 North College Avenue, Claremont, CA 91711, USA
[f] Institut für Anorganische Chemie, RWTH Aachen University, 52056 Aachen, Germany

ARTICLE INFO

Article history:
Received 18 May 2011
Received in revised form 10 September 2011
Accepted 17 October 2011
Available online 25 October 2011

Keywords:
Anti-cancer drugs
Triphenyltin(IV) benzoates
Triphenyltin(IV) 2-/4-[(*E*)-2-(aryl)-1-diazenyl]benzoates
Cell lines
QSAR

ABSTRACT

Four new triphenyltin(IV) complexes of composition Ph_3SnLH (where LH = 2-/4-[(*E*)-2-(aryl)-1-diazenyl] benzoate) (1–4) were synthesized and characterized by spectroscopic (^1H, ^{13}C and ^{119}Sn NMR, IR, ^{119}Sn Mössbauer) techniques in combination with elemental analysis. The ^{119}Sn NMR spectroscopic data indicate a tetrahedral coordination geometry in non-coordinating solvents. The crystal structures of three complexes, Ph_3SnL^1H (1), Ph_3SnL^3H (3), Ph_3SnL^4H (4), were determined. All display an essentially tetrahedral geometry with angles ranging from 93.50(8) to 124.5(2)°; ^{119}Sn Mössbauer spectral data support this assignment. The cytotoxicity studies were performed with complexes 1–4, along with a previously reported complex (5) *in vitro* across a panel of human tumor cell lines *viz*., A498, EVSA-T, H226, IGROV, M19 MEL, MCF-7 and WIDR. The screening results were compared with the results from other related triphenyltin(IV) complexes (6–7) and tributyltin(IV) complexes (8–11) having 2-/4-[(*E*)-2-(aryl)-1-diazenyl]benzoates framework. In general, the complexes exhibit stronger cytotoxic activity. The results obtained for 1–3 are also comparable to those of its *o*-analogs i.e. 4–7, except 5, but the advantage is the former set of complexes demonstrated two folds more cytotoxic activity for the cell line MCF-7 with ID_{50} values in the range 41–53 ng/ml. Undoubtedly, the cytotoxic results of complexes 1–3 are far superior to CDDP, 5-FU and ETO, and related tributyltin(IV) complexes 8–11. The quantitative structure-activity relationship (QSAR) studies for the cytotoxicity of triphenyltin (IV) complexes 1–7 and tributyltin(IV) complexes 8–11 is also discussed against a panel of human tumor cell lines.

1. Introduction

Organotin(IV) compounds are a widely studied class of metal-based anti-tumor drugs and their intensive investigation has led to the discovery of compounds with excellent *in vitro* anti-tumor activity, but in many cases disappointingly low *in vivo* potency or high *in vivo* toxicity [1–3]. It is well established that organotin(IV) compounds are very important in cancer chemotherapy because of their apoptosis-inducing character [4,5]. The design of improved organotin(IV) anti-tumor agents occupies a significant place in cancer chemotherapy, as revealed in their remarkable therapeutic potential reflected in recent research reports [6–17]. Consequently, a large number of organotin(IV) carboxylates have been investigated for their anti-tumor potential. Among organotin(IV) carboxylates, triorganotin(IV) carboxylates are quite well known for exceptionally high *in vitro* anti-tumor activities, *e.g.*, triphenyltin(IV) -benzoates, -salicylates [18], -3,6-dioxaheptanoate, -3,6,9-trioxadecanoate [19], -4-carboxybenzo-15-crown-5, -4-carboxybenzo-18-crown-6 [19,20], -steroidcarboxylate [21], -terebate [22,23,24] and -aminoacetates (Schiff bases) [25,26]. From these examples, it is clear that the compounds can be developed with high *in vitro* antitumor activity and sufficient water solubility. The most important point remains the activity. The organotin(IV) compounds containing the diazenyl group show not only high *in vitro* antitumor activity, but also displayed interesting interactions with various enzymes (see below). In the present study, attempts have been made to improve the water solubility by the systematic study of various

* Corresponding author. Tel.: +91 364 2722626; fax: +91 364 2721000.
E-mail addresses: basubaul@nehu.ac.in, basubaul@hotmail.com (T.S. Basu Baul), Rajeshwar.Verma@fda.hhs.gov, rajeshwarv@yahoo.com (R.P. Verma).
[1] Present address (Rajeshwar P. Verma): U.S. Food and Drug Administration, Center for Food Safety and Applied Nutrition, OFAS/OCAC, 5100 Paint Branch Parkway, College Park, MD 20740, USA.

0162-0134/$ – see front matter © 2011 Elsevier Inc. All rights reserved.
doi:10.1016/j.jinorgbio.2011.10.008

structural changes. In general, organotin(IV) compounds are dissolved in DMSO and diluted with test medium prior to the in vitro testing. The limited solubility needs further improvement in a way comparable to cisplatin which shows limited water solubility too.

In view of the remarkable activity of the triphenyltin(IV) carboxylates, triphenyltin(IV) carboxylates containing the 2-[(*E*)-2-(3-formyl-4-hydroxyphenyl)-1-diazenyl]benzoate and 2-[(*E*)-2-(4-hydroxy-5-methylphenyl)-1-diazenyl]benzoate skeletons have recently been investigated, showing encouraging cytotoxic activity across a panel of cell lines [27]. As a result of these promising cytotoxic activities, the mechanistic role of the compounds was investigated to determine the influence of the azo group nitrogen. Docking studies were performed with some of the key enzymes, such as ribonucleotide reductase, thymidylate synthase, thymidylate phosphorylase and topoisomerase II, which take part in the synthesis of raw materials for DNA and its replication [28]. The docking studies indicated that the azo group nitrogen atoms and formyl, carbonyl and ester oxygen atoms in the ligand moiety play an important role. They exhibit hydrogen bonding interactions with the active site of amino acids of the aforementioned enzymes. The higher activity was attributed to the presence of the azo group nitrogen atoms in the molecules of triphenyltin (IV) complexes [27]. As a continuation of our previous work in this area, we report some new triphenyltin(IV) complexes, $Ph_3SnL^{1-4}H$ (**1**–**4**), of related systems where the ligand skeletal framework has been modified (Scheme 1) in an attempt to improve the dissolution properties and thereby influence cytotoxicity. The carboxylate ligands selected herein have variations in the position of the carboxylate functionality in the diazo part and also have variations of the nuclear substituents in the coupling moieties of the molecule. The newly synthesized complexes (**1**–**4**) were characterized by spectroscopic (^{1}H, ^{13}C and ^{119}Sn NMR, IR, ^{119}Sn Mössbauer) techniques. Complete characterization was accomplished from the crystal structure determination of some representative complexes Ph_3SnL^1H (**1**), Ph_3SnL^3H (**3**) and Ph_3SnL^4H (**4**). The newly synthesized triphenyltin(IV) complexes (**1**–**4**) and one previously reported triphenyltin(IV) complexes Ph_3SnL^5H (**5**) [29] were tested across a panel of human tumor cell lines consisting of A498 (renal cancer), EVSA-T (mammary cancer), H226 (non-small-cell lung cancer), IGROV (ovarian cancer), M19 MEL (melanoma), MCF-7 (mammary cancer) and WIDR (colon cancer) and the results were compared with analogous Ph_3SnL^6H (**6**), Ph_3SnL^7H (**7**) [27] and related tributyltin(IV) complexes (**8**–**11**) (see Scheme 1 for complex description).

2. Experimental

2.1. Materials

Ph_3SnOH was prepared from Ph_3SnCl (Fluka) by following the literature method [30]. $(Ph_3Sn)_2O$ (Fluka), 2-hydroxybenzaldehyde (Sisco), 2-methylphenol, 4-methylphenol, 4-*tert*-butylphenol (Merck), anthranilic acid (Spectrochem), and 4-aminobenzoic acid (Hi Media) were used without further purification. The solvents used in the reactions were of AR grade and were dried using standard procedures. Toluene was distilled from sodium benzophenone ketyl.

2.2. Physical measurements

Carbon, hydrogen and nitrogen analyses were performed with a Perkin Elmer 2400 series II instrument. IR spectra in the range 4000–400 cm^{-1} were obtained on a Perkin Elmer Spectrum BX series FT-IR spectrophotometer with samples investigated as KBr disks. The ^{1}H and ^{13}C spectra were recorded on a Bruker AMX 400 spectrometer and measured at 400.13 and 100.62 MHz, respectively, while ^{119}Sn NMR spectra were recorded on a Jeol GX 270 spectrometer and measured at 100.75 MHz. The ^{1}H, ^{13}C and ^{119}Sn chemical shifts were referenced to Me_4Si, $CDCl_3$ and Me_4Sn set at 0.00, 77.0 and 0.00 ppm, respectively. The ^{119}Sn Mössbauer spectra (Table 1) were recorded at liquid nitrogen temperature with a conventional instrument in transmission mode, constituted by a multichannel analyzer (TAKES Mod.269, Ponteranica, Italy) and the following Wissenschaftliche Elektronik system (MWE, München, Germany): MR250 driving unit, FG2 digital function generator and MA250 velocity transducer, moving at linear velocity, constant acceleration, in a triangular waveform. The organotin(IV) samples (**1**–**4**) were maintained at liquid nitrogen temperature in a Cryo NDR-1258-MD liquid nitrogen cryostat (Cryo Industries of America, Inc. Atkinson, NH, USA) with a Cryo sample holder. The 77.3 ± 0.1 K temperature was controlled with an Oxford Instruments ITC 502 temperature controller (Oxford, UK). The multichannel calibration was performed with an enriched iron foil (α^{57}Fe, 4 μm thick, RITVERC GmbH, St. Petersburg, Russia), at room temperature, by using a ^{57}Co/Rh source (10 mCi, RITVERC GmbH, St. Petersburg, Russia), while the zero point of the Doppler velocity scale was determined, at room temperature, through absorption spectra of natural $CaSnO_3$ (^{119}Sn = 0.5 mg cm^{-2}) and a $Ba^{119}SnO_3$ source (10 mCi, RITVERC GmbH). The obtained $5 \cdot 10^5$ count spectra were interpreted by means of non-linear least square analysis as a sum of Lorentzian doublets, to obtain the isomer shift, $\delta \pm 0.03$ mm s^{-1}, the nuclear quadrupole splitting, $|\Delta_{exp}| \pm 0.03$ mm s^{-1} and the average full width at half height, Γ_{av}, ± 0.03 mm s^{-1}.

2.3. Synthesis of ligands and complexes

Ligands 4-[(*E*)-2-(4-hydroxy-3-methylphenyl)-1-diazenyl]benzoic acid (L^2HH') [31], 4-[(*E*)-(5-*tert*-butyl-2-hydroxyphenyl)diazenyl]benzoic acid (L^3HH') [31,32], 2-[(*E*)-(5-*tert*-butyl-2-hydroxyphenyl)diazenyl]benzoic acid (L^4HH') [31,33], and complex **5** [29] were prepared by the methods described in our earlier reports and purities were established from melting point, elemental analysis and ^{1}H NMR spectroscopy.

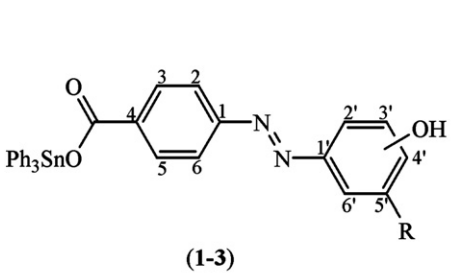

(1-3)

L^1H = 2'-OH, R = Me : Ph_3SnL^1H (**1**)
L^2H = 4'-OH, R = Me : Ph_3SnL^2H (**2**)
L^3H = 2'-OH, R = t-Bu : Ph_3SnL^3H (**3**)

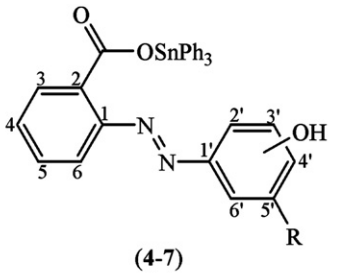

(4-7)

L^4H = 2'-OH, R = t-Bu : Ph_3SnL^4H (**4**)
L^5H = 2'-OH, R = Me : Ph_3SnL^5H (**5**)
L^6H = 4'-OH, R = Me : Ph_3SnL^6H (**6**)
L^7H = 4'-OH, R = CHO : Ph_3SnL^7H (**7**)

Scheme 1. Structures and numbering protocol of triphenyltin(IV) complexes $Ph_3SnL^{1-7}H$ (**1**–**7**).

Table 1
Experimental[a] and calculated Mössbauer parameters, including C-Sn-O angles for the triphenyltin(IV) complexes **1–4.**

Complex	δ	$\|\Delta_{exp}\|$	Γ_{av}	$\Delta_{calcd.}$[b]	C-Sn-O angle
1	1.17	2.27	0.76	−2.22	109.07
2	1.19	2.24	0.84	−2.22	109.31
3	1.16	2.44	0.99	−2.22	107.63
4	1.16	2.40	0.96	−2.22	107.98

[a] Conditions: 77 K, 0.50–0.60 mg cm^{-2} ^{119}Sn. δ, Δ, and Γ values are in mm s^{-1} and angles are in degrees, and the errors limits are ±0.03 mm s^{-1} and 13°, respectively.
[b] Calculated assuming a regular tetrahedral structure. Used partial quadrupole splitting (p.q.s.) values (mm s^{-1}): {Ph} = −1.26 [51], $\{COO^-\}_{unid}$ = −0.15[51].

2.3.1. Synthesis of 4-[(E)-2-(2-hydroxy-5-methylphenyl)-1-diazenyl] benzoic acid (L^1HH')

Ligand L^1HH' was prepared by reacting *p*-carboxybenzenediazonium chloride with 4-methylphenol in alkaline solution under cold conditions, following the method described for its *o*-analog L^5HH' [29]. Several recrystallizations from hot methanol yielded an orange crystalline product in 60% yield; M.p.: 260–261 °C. Anal. Calc. for $C_{14}H_{12}N_2O_3$: C, 65.62; H, 4.72; N, 10.93%. Found. C, 65.28; H, 4.65; N, 10.85%. IR absorption (cm^{-1}): 1680 $\nu(OCO)_{as}$. ^{1}H-NMR (DMSO-d_6): δ H: 8.19 [dd, 2.5 Hz, 8.0 Hz, 2H, H2/6], 7.91 [dd, 2.5 Hz, 8.0 Hz, 2H, H3/5], 7.75 [d, 2.5 Hz, 1H, H6′], 7.20 [dd, 2.5, 8 Hz, 1H, H4′], 6.93 [d, 8 Hz, 1H, H3′], 2.39 [s, 3H, CH_3] ppm. Signal for carboxylic and phenolic protons were exchanged due to presence of water in the solvent. ^{13}C-NMR (DMSO-d_6); δ C: 167.1 [CO_2], 19.7 [CH_3], other carbons: 152.6, 150.1, 136.7, 134.6, 132.3, 130.4, 128.9, 121.4, 117.4 ppm.

2.3.2. Synthesis of Ph_3SnL^1H (**1**)

Complex **1** was synthesized by reacting L^1HH' (0.30 g, 1.17 mmol) and $(Ph_3Sn)_2O$ (0.42 g, 0.59 mmol) in anhydrous toluene (40 ml) in a 100 ml flask equipped with a Dean-Stark moisture trap and water-cooled condenser. The reaction mixture was refluxed for 9 h and filtered while hot. The filtrate was collected and the volatiles removed using a rotary evaporator. The residue was dried *in vacuo*, washed with hexane (3 × 5 ml), extracted into benzene and filtered. The filtrate was concentrated and petroleum ether added to precipitate the crude product, which was collected by filtration and dried *in vacuo* (m.p.: 152–154 °C). Recrystallization from benzene gave maroon crystals of the desired product in 55% (0.40 g) yield. M.p.: 168–170 °C. Anal. Calc. for $C_{32}H_{26}N_2O_3Sn$: C, 63.48; H, 4.33; N, 4.63%. Found. C, 64.28; H, 4.45; N, 4.70%. IR absorption (cm^{-1}): 1624 $\nu(OCO)_{as}$. ^{1}H-NMR ($CDCl_3$): δ H: 12.6 [brs, 1H, OH], 8.26 [dd, 2.5 Hz, 8.0 Hz, 2H, H2/6], 7.87 [dd, 2.5 Hz, 8.0 Hz, 2H, H3/5], 7.84 [m, 6H, Sn-Ph_o], 7.72 [d, 2.5 Hz, 1H, H6′], 7.46 [m, 9H, Sn-$Ph_{m/p}$], 7.14 [dd, 2.5, 8 Hz, 1H, H4′], 6.91 [d, 8 Hz, 1H, H3′], 2.35 [s, 3H, CH_3] ppm. ^{13}C-NMR ($CDCl_3$); δ C: 172.2 [CO_2], 138.6 [Sn-Ph_i], 137.4 [Sn-Ph_o], 130.7 [Sn-Ph_p], 129.5 [Sn-Ph_m], 20.7 [CH_3], other carbons: 153.6, 151.2, 135.6, 133.7, 133.0, 132.3, 129.8, 122.3, 118.5 ppm.^{119}Sn-NMR ($CDCl_3$): −104.6 ppm.

2.3.3. Synthesis of Ph_3SnL^2H (**2**)

Ph_3SnOH (0.43 g, 1.17 mmol) was dissolved in anhydrous benzene and added to an anhydrous methanol solution containing L^2HH' (0.30 g, 1.17 mmol). The reaction mixture was refluxed for 6 h and the water formed during the reaction being removed azeotropically using a Dean-Stark apparatus. The reaction mixture was filtered while hot and the filtrate was evaporated to dryness using a rotary evaporator. The dried mass was washed thoroughly with hexane, extracted into anhydrous benzene and filtered. The filtrate was concentrated slowly on a hot plate, cooled to room temperature and solid precipitated with hexane. The crude product was collected by filtration, washed several times with hot hexane and recrystallized using benzene to afford yellow crystalline material in 45% (0.33 g) yield. M.p.: 148–150 °C. Anal. Calc. for $C_{32}H_{26}N_2O_3Sn$: C, 63.48; H, 4.33; N, 4.63%. Found. C, 63.50; H, 4.45; N, 4.45%. IR absorption (cm^{-1}): 1608 $\nu(OCO)_{as}$. ^{1}H-NMR (DMSO-d_6); δ H: 9.60 [brs, 1H, OH], 8.95 [dd, 2.5 Hz, 8.0 Hz, 2H, H2/6], 7.88 [m, 6H, Sn-Ph_o], 7.77 [dd, 2.5 Hz, 8.0 Hz, 2H, H3/5], 7.68 [d, 2.5 Hz, 1H, H6′], 7.61 [dd, 2.5, 8 Hz, 1H, H2′], 7.40 [m, 9H, Sn-$Ph_{m/p}$], 6.88 [d, 8 Hz, 1H, H5′], 2.26 [s, 3H, CH_3] ppm. ^{13}C-NMR (DMSO-d_6); δ C: 168.5 [CO_2], 141.7 [Sn-Ph_i], 135.5 [Sn-Ph_o], 127.8 [Sn-Ph_p], 127.2 [Sn-Ph_m], 15.3 [CH_3], other carbons: 158.6, 153.3, 144.6, 129.6, 124.1, 123.9, 122.8, 120.7, 113.8 ppm. ^{119}Sn-NMR ($CDCl_3$): −105.6 ppm.

2.3.4. Synthesis of Ph_3SnL^3H (**3**)

Complex **3** was prepared by reacting Ph_3SnOH with L^3HH' using the procedure described for **2** in anhydrous toluene. Dried residue was extracted in chloroform, concentrated, precipitated with hexane and filtered. The crude product was dried and recrystallized with acetone, affording orange crystalline material in 56% yield. M.p.: 130–132 °C. Anal. Calc. for $C_{35}H_{32}N_2O_3Sn$: C, 64.92; H, 4.98; N, 4.33%. Found. C, 65.08; H, 4.85; N, 4.35%. IR absorption (cm^{-1}): 1621 $\nu(OCO)_{as}$. ^{1}H-NMR ($CDCl_3$): δ H: 12.5 [brs, 1H, OH], 8.26 [dd, 2.5 Hz, 8.0 Hz, 2H, H2/6], 7.87 [m, 3H, H3/5/6′], 7.78 [m, 6H, Sn-Ph_o], 7.45 [m, 10H, Sn-$Ph_{m/p}$/H4′], 6.91 [d, 8 Hz, 1H, H3′], 1.31 [s, 9H, CH_3] ppm. ^{13}C-NMR ($CDCl_3$); δ C: 171.6 [CO_2], 138.1 [Sn-Ph_i], 136.8 [Sn-Ph_o], 131.8 [Sn-Ph_p], 128.8 [Sn-Ph_m], 30.3 [CH_3], other carbons: 153.0, 150.7, 142.4, 136.7, 130.0, 129.9, 121.6, 117.8 ppm. ^{119}Sn-NMR ($CDCl_3$): −104.6 ppm.

2.3.5. Synthesis of Ph_3SnL^4H (**4**)

Complex **4** was prepared by reacting Ph_3SnOH with L^4HH' by following an analogous procedure described for complex **3**. The product was recrystallized from chloroform to afford orange crystals in 76% yield. M.p.: 138–140 °C. Anal. Calc. for $C_{35}H_{32}N_2O_3Sn$: C, 64.92; H, 4.98; N, 4.33%. Found. C, 65.18; H, 4.90; N, 4.35%. IR absorption (cm^{-1}): 1606 $\nu(OCO)_{as}$ ^{1}H-NMR ($CDCl_3$): δ H: 12.7 [brs, 1H, OH], 8.22 [d, 8 Hz, 1H, H3], 7.84 [m, 8H, Sn-Ph_o/H6/H6′], 7.56 [t, 8 Hz, 1H, H5], 7.42 [m, 11H, Sn-$Ph_{m/p}$/H4/H4′], 6.96 [d, 8 Hz, 1H, H3′], 1.37 [s, 9H, CH_3] ppm. ^{13}C-NMR ($CDCl_3$); δ C: 171.3 [CO_2], 137.1 [Sn-Ph_i], 136.0 [Sn-Ph_o], 129.0 [Sn-Ph_p], 127.7 [Sn-Ph_m], 30.3 [CH_3], other carbons: 149.5, 149.4, 140.9, 136.3, 131.7, 131.6, 130.0, 128.9, 128.7, 127.1, 126.1, 117.2, 114.9 ppm. ^{119}Sn-NMR ($CDCl_3$): −104.2 ppm.

2.4. Experimental protocol and cytotoxicity tests

The *in vitro* cytotoxicity testing of triphenyltin(IV) complexes **1–5** was performed using the SRB test for estimation of cell viability. Experimental protocols for **6** and **7** have been reported [27] and the cytotoxic results are included here for convenience of discussion. The cell lines WIDR colon carcinoma, M19 MEL melanoma, A498 renal cell carcinoma, IGROV ovarian carcinoma and H226 non-small-cell lung cancer belong to the currently used anticancer screening panel of the NCI, USA [34]. The breast carcinoma MCF7 cell line is estrogen receptor (ER)+/progesterone receptor (PgR)+ and the breast carcinoma cell line EVSA-T is (ER)-/(Pgr)-. Prior to the experiments, a mycoplasma test was carried out on all cell lines and found to be negative. All cell lines were maintained in a continuous logarithmic culture in RPMI 1640 medium with HEPES and phenol red. The medium was supplemented with 10% FCS, penicillin 100 μg/ml and streptomycin 100 μg/ml. The cells were mildly trypsinized for passage and for use in the experiments. RPMI and FCS were obtained from Life Technologies or from Gibco (Paisley, Scotland). SRB, DMSO, penicillin and streptomycin were obtained from Sigma (St. Louis MO, USA), TCA and acetic acid from Baker BV (Deventer, NL) and PBS from NPBI BV (Emmer-Compascuum, NL).

The test complexes **1–5** and reference compounds were dissolved to a concentration of 250,000 ng/ml in full medium, by dilution of a stock solution which contained 5 mg of complexes **1–5**/ml in DMSO. (Note: Complex **1** did not dissolve well in DMSO and hence needed stirring at 37 °C and then at 50 °C, but it still did not dissolve

completely and therefore a suspension of the test complex **1** in DMSO was used to make the dilutions in medium). The compounds were subsequently diluted to a final concentration of 250,000 ng/ml in full medium. Cytotoxicity was estimated by the microculture sulforhodamine B (SRB) test [35].

The experiment was started on day 0. On day 0, 1500–2000 cells per well were seeded into 96-wells flat-bottomed micro-titer plates (Cellstar, Greiner Bio-one). The plates were pre-incubated overnight at 37 °C, 5% CO_2 to allow the cells to adhere to the bottom. On day 2, a three-fold dilution sequence of ten steps was made in full medium, starting with the 250,000 ng/ml stock solution. Every dilution was used in quadruplicate by adding 50 μl to a column of four wells. This procedure results in the highest concentration of 62,500 ng/ml being present in column 12. Column 2 was used for the blank.

Medium was added to column 1 to diminish interfering evaporation. On day 7, the incubation was terminated. Subsequently, the cells were fixed with 10% trichloroacetic acid in PBS and placed at 4 °C for an hour. After three washings with tap water, the cells were stained for at least 15 min with 0.4% SRB dissolved in 1% acetic acid. After staining, the cells were washed with 1% acetic acid to remove the unbound stain. The plates were air-dried and the bound stain was dissolved in 150 μl 10 mM Tris-base. The absorbance was measured at 540 nm using an automated microplate reader (Labsystems Multiskan MS). The data were used for construction of concentration-response curves and determination of the ID_{50} values by use of Deltasoft 3 software. ID_{50} is the dose in ng/ml that causes 50% inhibition of the tumor cells.

The variability of the *in vitro* cytotoxicity test depends on the cell lines used and the serum applied. With the same batch of cell lines and the same batch of serum the inter-experimental CV (coefficient of variation) is 1–11% depending on the cell line and the intra-experimental CV is 2–4%. These values may be higher in the other batches of cell lines and/or serum.

2.5. Quantitative structure-activity relationship (QSAR) methods

QSAR models were developed by the C-QSAR program [36] using multi-regression analyses (MRA). This program avoids the collinearity problem by auto-selection of descriptors based on permutation and correlation matrices among the descriptors. Details about this program and its use in the development of QSAR models can be seen in previous publications [37,38]. The *in vitro* cytotoxicity data (ID_{50}; ng/ml) of organotin(IV) compounds **1**–**20** along with some standard drug molecules against a panel of seven human tumor cell lines are summarized in Table 5. In QSAR analysis, we often like to convert the concentration ID_{50} of the compound into an activity parameter "A" using the following equation $A = -\log ID_{50} = \log 1/ID_{50}$ in molar concentration. This transformation represents that the more potent compound always has a higher "activity" and vice versa [39,40]. This is the reason the *in vitro* cytotoxicity data (ID_{50}; ng/ml) (see Table 5) was converted into an activity parameter log $1/ID_{50}$ (mol l^{-1}) using the following equation: log $1/ID_{50}$ (mol l^{-1}) = 6 − log [ID_{50} (ng/ml)/MW] and then the QSAR models were developed. Clog P is the calculated partition coefficient of a compound in octanol/water system and is a measure of its hydrophobicity, while CMR is the calculated molar refractivity for the whole molecule [36,41].

In all QSAR models, n is the number of data points, r^2 is the square of the correlation coefficient, q^2 is the cross-validated r^2, s is the standard deviation, Q is the quality factor, and F is the Fischer ratio. The cross-validated r^2 (q^2) is obtained by using the leave-one-out (LOO) procedure [42]. In each QSAR model, the value of F in parenthesis refers to their literature value at 95% level [43]. The modeling was taken to be optimal when Q reached a maximum together with F, even if slightly non-optimal F values have normally been accepted. A compound was assigned as an outlier on the basis of deviation between observed and predicted activities from the respective QSAR model [log $1/ID_{50}$ (obsd) − log $1/ID_{50}$ (pred)] > 2 s, where s is the standard deviation [41,44]. Each QSAR model includes 95% confidence limits for each term in parentheses. Statistical diagnostics (r^2, q^2, s, Q, and F) and internal validation (cross validation and Y-randomization) tests have validated all the QSAR models. Due to the small data sets, we did not perform the external validation test.

2.6. X-ray crystallography

Crystals of the triphenyltin(IV) complexes Ph_3SnL^1H (**1**), Ph_3SnL^3H (**3**) and Ph_3SnL^4H (**4**) suitable for single crystal X-ray structure determination were obtained from slow evaporation of benzene, acetone and chloroform solutions of the complexes, respectively. Intensity data were collected with graphite-monochromated MoKα radiation (λ = 0.71073 Å) on a Bruker D8 goniometer equipped with a SMART APEX CCD detector. Frames were collected in ω-scan mode and integrated with the help of the program SAINT [45]. Crystal data, data collection parameters and convergence results are listed in Table 2. Absorption corrections based on a multi-scan approach [46] were applied to the data sets before averaging over symmetry-related reflections. The structures were solved by direct methods with the help of the program SHELXS-97 [47] and refined on reflection intensities F^2 using SHELXL-97 [47]. In the final least-squares refinements, non-hydrogen atoms were refined with anisotropic displacement parameters and hydrogen atoms were placed in idealized positions and included as riding on the corresponding atoms.

The quality of the intensity data sets varied considerably: only room temperature data were available for **1**. 18 distance restraints and 656 rigid-bond restraints were used during refinement, and reliability factors were rather high. In the case of **3**, low temperature (130 (2) K) data were available; in each of the two symmetrically independent molecules one of the phenyl rings attached to the metal was disordered over two orientations; a total of 144 restraints were employed in the final structure model, and partially occupied atom

Table 2
Crystal data, data collection parameters and convergence results for complexes **1**, **3** and **4**.

	1	**3**	**4**
Empirical formula	$C_{32}H_{26}N_2O_3Sn$	$C_{35}H_{32}N_2O_3Sn$	$C_{35}H_{32}N_2O_3Sn$
Formula weight	605.24	647.32	647.32
Crystal size (mm)	0.30 × 0.15 × 0.15	0.42 × 0.23 × 0.03	0.28 × 0.18 × 0.04
Crystal morphology	Rod	Platelet	Platelet
Temperature (K)	293(2)	130(2)	110(2)
Crystal system	Triclinic	Triclinic	Triclinic
Space group	$P\bar{1}$	$P\bar{1}$	$P\bar{1}$
a (Å)	11.580(2)	9.6709(10)	9.8449(6)
b (Å)	12.288(3)	14.5077(15)	10.4548(7)
c (Å)	20.158(4)	21.438(2)	14.9268(10)
α (°)	98.265(5)	92.255(2)	97.600(2)
β (°)	94.693(4)	95.299(2)	92.305(2)
γ (°)	92.866(4)	92.960	104.383(2)
V (Å^3)	2823.5(10)	2988.0(5)	1470.86(17)
Z	4	4	2
Dx (g cm^{-3})	1.424	1.439	1.462
μ (mm^{-1})	0.939	0.893	0.907
Transmission factors (min, max)	0.765,0.872	0.705, 0.973	0.782, 0.964
θ range (°)	1.68–25.57	2.1–28.59	2.28–30.56
Reflections measured	16,377	31,236	21,927
Independent reflections; Rint	10,478; 0.0692	14,959; 0.0632	8347; 0.0612
Reflections with $I > 2\sigma(I)$	10,478	14,959	8347
Number of parameters	687	737	373
Number of restraints	674	144	0
$R(F)$ [$I > 2\sigma(I)$reflns]	0.070	0.081	0.038
$wR(F2)$ (all data)	0.212	0.110	0.048
GOF(F^2)	1.05	1.284	1.00
$\Delta\rho$max, min (e, Å^{-3})	0.67, −0.57	0.97, −1.31	1.39, −0.82

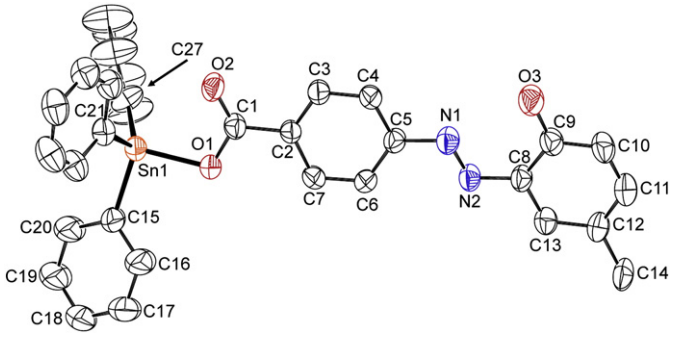

Fig. 1. Displacement ellipsoid plot (30% probability) showing one of the two independent molecules in the crystal of Ph_3SnL^1H (**1**) with the atom-labeling scheme. Hydrogen atoms have been omitted for clarity.

sites were assigned isotropic displacement parameters. Refinement of **4** was straightforward.

3. Results and discussion

3.1. Synthesis and spectroscopy

Ligands L^1HH'-L^5HH' were prepared by reacting the appropriate *ortho*-/*para*-carboxybenzenediazonium chloride with 2-methylphenol, 4-methylphenol or 4-*tert*-butylphenol in alkaline solution under cold conditions [27,29,31,32]. Reactions of the ligand with $(Ph_3Sn)_2O$ or Ph_3SnOH in a suitable solvent (see experimental section for details) after proper work-up afforded triphenyltin(IV) complexes of composition Ph_3SnLH with yields greater than 45%. The compounds are colored solids that are air stable and soluble in all common organic solvents. Analytical purities of the complexes were established by elemental analyses and multinuclear NMR (^{1}H, ^{13}C and ^{119}Sn) spectroscopic data.

The IR spectra of the triphenyltin(IV) complexes displayed a strong sharp band at around 1620 cm^{-1} (for **1** and **3**) and 1605 cm^{-1} (for **2** and **4**) that has been assigned to the asymmetric carboxylate [$\nu(OCO)_{as}$] stretching vibration, in accord with our earlier reports [27,29,31,48]. The assignment of the symmetric [$\nu(OCO)_{sym}$] stretching vibration band could not be made owing to the complex spectral pattern. All complexes displayed ^{1}H and ^{13}C signals due to ligand and Sn-Ph skeletons. The observed ^{1}H- and ^{13}C-NMR signals are given in the experimental section. The ^{1}H-NMR integration values were completely consistent with the formulation of the products. The ^{1}H and ^{13}C chemical shift assignment of the phenyltin moiety is straightforward from the multiplicity patterns, resonance intensities and also by examining the $^nJ(^{13}C\text{-}^{119/117}Sn)$ coupling constants [29,48,49]. In $CDCl_3$, the triphenyltin(IV) complexes (**1**–**4**) exhibit a single sharp ^{119}Sn resonance at around −105 ppm, suggesting that the Sn-atom in the complexes are isostructural in solution where the tin atom is four-coordinate [27,29,49,50]. ^{119}Sn Mössbauer

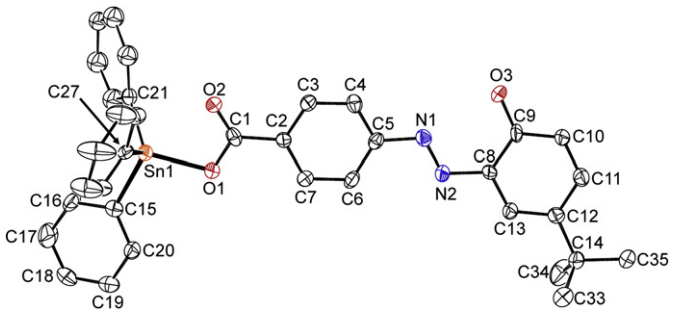

Fig. 2. Displacement ellipsoid plot (50% probability) showing one of the two independent molecules in the crystal of Ph_3SnL^3H (**3**) with the atom-labeling scheme. Hydrogen atoms and an alternative minority conformation for one of the phenyl rings have been omitted for clarity.

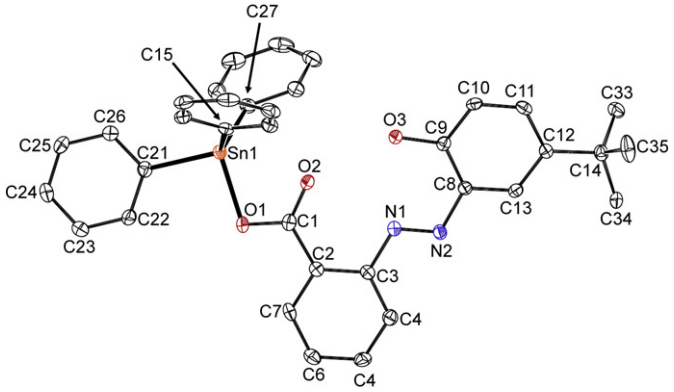

Fig. 3. Displacement ellipsoid plot (50% probability) of a molecule in the crystal of Ph_3SnL^4H (**4**) with the atom-labeling scheme. Hydrogen atoms have been omitted for clarity.

data can usually give information on the more or less covalent nature of the bonds formed by tin with other and different atoms through determination of the isomer shift values, δ, and also an insight into the probable structure of the complexes, both in the solid state or in frozen solution, by the determination of experimental nuclear quadrupole splittings, $|\Delta_{exp}|$. The experimental Mössbauer spectra show, in all the cases, a single resonant doublet with full width at half height broader than that of the $Ba^{119}SnO_3$ source (~1 mm s^{-1}) (see Γ_{av} in Table 1), which is consistent with the occurrence of only one absorbing species. The experimental Mössbauer parameters are reported in Table 1, together with calculated Δ according to the point-charge model formalism applied to the idealized tetrahedral structure [51–56]. The difference between experimental and calculated values does not exceed the limit of tolerance of the method (±0.4 mm s^{-1}) [55], and thus the experimental $|\Delta_{exp}|$ data can be explained satisfactorily by assuming a slightly distorted tetrahedral geometry [56]. As a consequence, taking into account the proposed tetracoordination of tin(IV) and using the Parish equation, the calculated C–Sn–OCO angles for the complexes **1**–**4** lie in the range 107.6–109.3° [56] (see Table 1).

3.2. Crystal structures

The crystal structures of three of the triphenyltin complexes (**1**, **3** and **4**) have been determined. Crystal data, data collection parameters and refinement results are given in Table 2. All three complexes crystallize in the triclinic space group $P\bar{1}$. The crystal structures of **1** and **3** feature two independent molecules in the asymmetric unit. Views of the molecules of **1**, **3** and **4** are shown in Figs. 1–3. With respect to the metal coordination, the structures conform to the same motif. Selected geometric parameters are given in Table 3. As indicated by the ^{119}Sn Mössbauer spectroscopy, the molecules are monomeric in the solid state. The tin atom is four coordinate with a distorted tetrahedral geometry defined by a C_3O donor set. The tetrahedral angles for the five molecules range between 93.50(8) and 124.5(2)°. Similar tetrahedral geometries about the Sn atom were observed in $Ph_3Sn[O_2CC_6H_4(N=NC_6H_3\text{-}2\text{-}OH\text{-}5\text{-}Me)\text{-}o]$ and its acetone solvated complex [57,58], $Ph_3Sn\{O_2CC_6H_3\text{-}p\text{-}OH[N=N(C_6H_4\text{-}X)]\}$ X = H, 2-Me, 3-Me, 4-Me, 4-OMe, 4-Cl [50,59,60] and $Bu_3Sn[O_2CC_6H_4(N=NC_6H_3\text{-}4\text{-}OH\text{-}5\text{-}Me)\text{-}p]$ [61]. The fifth potential donor atom, O(2), remains at a significantly longer distance from the tin center than O(1), with values between 2.564(2) and 2.862(7) Å. In agreement with the different metal-oxygen distances, C(1)-O(1) bonds are consistently longer than the C(1)-O(2) distances (Table 3). The secondary Sn-O(2) interaction causes a slight distortion of the tetrahedral primary coordination sphere but should not be regarded as a strong coordinative bond: The bond angles around the Sn atom in **1**, **3** and **4** are more consistent with a tetrahedral environment than with a trigonal bipyramidal or square-pyramidal five-coordinate arrangement, and the

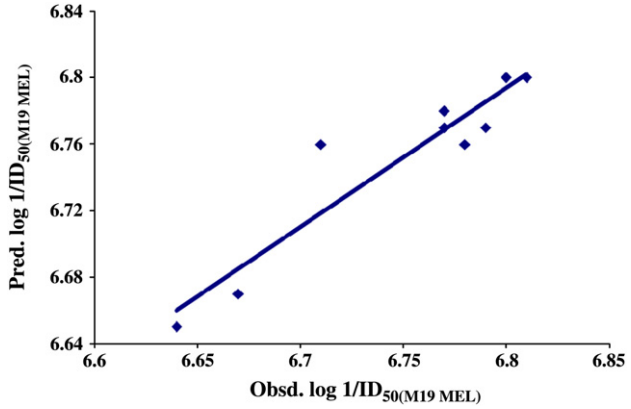

Fig. 4. Plot of observed log $1/ID_{50(M19\ MEL)}$ versus predicted log $1/ID_{50(M19\ MEL)}$ from QSAR 5 (Table 6).

same hypothesis was drawn from the ^{119}Sn Mössbauer data (*vide supra*). Compounds **1**, **3** and **4** represent typical van der Waals crystals without strong directional intermolecular contacts (Table 4). In all three compounds, the hydroxy oxygen atom O(3) acts as the donor and N(1) as the acceptor of an intramolecular hydrogen bond with graph set symbol *S*(6) [62]. As a result of the 1, 2 substitution in the aromatic ring C(2)-C(7), molecules of **4** adopt a more compact conformation than those in **1** and **3**. The packing diagrams for **1**, **3** and **4** can be viewed in Figs. S1–S3.

3.3. Cytotoxicity studies

Triphenyltin(IV) 2-[(*E*)-2-(aryl)-1-diazenyl]benzoates, *e.g.* **6**–**7**, are an important class of compounds as they have shown both effective docking results, particularly the hydrogen bonding interactions through the azo group nitrogen atoms, formyl, carbonyl and ester oxygen atoms with various key enzymes, and cytotoxic potential [27].

Table 3
Selected geometric parameters (Å, °)[a] for the triphenyltin(IV) complexes **1**, **3** and **4**.

	1	3	4
Sn(1)–O(1)	2.053(5)	2.079(4)	2.094(2)
[Sn(1a)–O(1a)]	[2.058(6)]	[2.072(4)]	
Sn(1)–O(2)	2.749(6)	2.655(4)	2.564(2)
[Sn(1a)-O(2a)]	[2.862(7)]	[2.775(4)]	
Sn(1)–C(15)	2.067(10)	2.140(6)	2.135(2)
[Sn(1a)–C(15a)]	[2.085(11)]	[2.136(6)]	
Sn(1)–C(21)	2.107(10)	2.109(7)	2.140(2)
[Sn(1a)–C(21a)]	[2.069(10)]	[2.135(6)]	
Sn(1)–C(27)	2.042(10)	2.109(7)	2.126(2)
[Sn(1a)–C(27a)]	[2.074(11)]	[2.115(7)]	
O(1)–C(1)	1.321(10)	1.326(7)	1.304(3)
[O(1a)–C(1a)]	[1.309(11)]	[1.318(7)]	
O(2)–C(1)	1.221(10)	1.237(8)	1.239(3)
[O(2a)–C(1a)]	[1.217(11)]	[1.220(7)]	
O(1)–Sn(1)–O(2)	52.7(2)	54.57(15)	54.93(6)
[O(1a)–Sn(1a)–O(2a)]	[50.1(2)]	[52.22(15)]	
O(1)–Sn(1)–C(15)	95.0(3)	100.5(2)	111.53(8)
[O(1a)–Sn(1a)–C(15a)]	[94.4(4)]	[93.9(2)]	
O(1)–Sn(1)–C(21)	111.3(3)	111.3(2)	93.50(8)
[O(1a)–Sn(1a)–C(21a)]	[108.4(3)]	[109.3(2)]	
O(1)–Sn(1)–C(27)	109.2(3)	111.1(2)	112.27(8)
[O(1a)–Sn(1a)–C(27a)]	[110.1(3)]	[104.4(2)]	
C(15)–Sn(1)–C(21)	109.1(4)	105.0(2)	107.12(9)
[C(15a)–Sn(1a)–C(21a)]	[112.1(5)]	[112.3(2)]	
C(15)–Sn(1)–C(27)	110.0(4)	109.4(2)	118.06(9)
[C(15a)–Sn(1a)–C(27a)]	[111.9(5)]	[107.7(2)]	
C(21)–Sn(1)–C(27)	119.5(4)	117.9(2)	111.52(9)
[C(21a)–Sn(1a)–C(27a)]	[117.4(5)]	[124.5(2)]	
C(1)–O(1)–Sn(1)	107.9(6)	104.4(4)	103.29(14)
[C(1a)–O(1a)–Sn(1a)]	[112.1(7)]	[107.9(4)]	

[a] Values in square brackets with the atom label extension 'a' refer to the second independent molecule in the asymmetric unit.

Table 4
Hydrogen bonding geometry (Å, °) for **1**, **3** and **4.**

Compound	D-H···A	D-H	H···A	D···A	D-H···A
1 Molecule 1[a]	O(3)-H(3O)···N(1)	0.82	1.87	2.569(11)	143
Molecule 2[a]	O(3A)-H(3P)···N(1A)	0.82	1.90	2.600(10)	142
3 Molecule 1[a]	O(3)-H(3O)···N(1)	0.84	1.92	2.628(7)	142
Molecule 2[a]	O(3A)-H(3P)···N(1A)	0.84	1.90	2.608(6)	141
[b]	O(3)-H(3O)···O(3)[i]	0.84	2.54	2.843(6)	102
4 [a]	O(3)-H(3O)···N(1)	0.84	1.90	2.598(3)	140
[b]	O(3)-H(3O)···O(2)	0.84	2.12	2.777(2)	135

"i" refers to atoms from the next symmetrically-related molecule (symmetry code: -x,2-y,-z).
[a] Intramolecular H-bond.
[b] Intermolecular H-bond (longer and weaker).

Such delicate bonding interactions are regulated by the geometrical features, size and presence of the donor atoms in the molecule. In view of this, some new triphenyltin(IV) 4-[(*E*)-2-(aryl)-1-diazenyl]benzoates (**1**–**3**) have been prepared by controlling and confining the parameters described above. These complexes were tested for their cytotoxic potential, along with two more triphenyltin(IV) 2-[(*E*)-2-(aryl)-1-diazenyl]benzoates (**4**–**5**), across the panel of human tumor cell lines A498, EVSA-T, H226, IGROV, M19 MEL, MCF-7 and WIDR. The results of the *in vitro* cytotoxicity tests performed with triphenyltin(IV) complexes (**1**–**5**) are summarized in Table 5 and the screening results are compared with the results from other related triphenyltin(IV) complexes (**6**–**7**) and tributyltin(IV) complexes (**8**–**11**) having 2-/4-[(*E*)-2-(aryl)-1-diazenyl]benzoates framework. Subsequently, the results were evaluated with the triphenyltin(IV)- 2-{[(2*Z*)-(3-hydroxy-1-methyl-2-butenylidene)]amino}-4-methyl-pentanoate, 2-{[(*E*)-1-(2-hydroxyphenyl)alkylidene]amino}-4-methyl-pentanoates, 2-{[(2*Z*)-(3-hydroxy-1-methyl-2-butenylidene)]amino}phenylpropionate, 2-{[(*E*)-1-(2-hydroxyphenyl)alkylidene]amino}phenylpropionate (**12**–**17**) [25,26], terebate, steroidcarboxylate and benzocrowncarboxylate (**18**–**20**) [23], which have shown promising activity. When looking into the antitumor test results of triorganotin(IV) derivatives, the question of hydrolysis yielding *e.g.* triphenyltin hydroxide as an active species may arise. The potent and similar *in vitro* activity of triphenyltin(IV) benzoates suggested triphenyltin hydroxide as the common intermediate responsible for cytotoxicity [63] and this hypothesis was also proposed for a series of dioxastannolanes. Later, this proposal was abandoned because of the observed resistance in the cell lines which was not seen with triphenyltin hydroxide [64]. Organotin(IV) carboxylates proved to be stable at least for days in water [65]. In our test system, either ethanol or DMSO solution of the organotin(IV) compound is diluted with test medium. In case of compounds insoluble in aqueous media, the test procedure is discontinued because of improper outcomes. Consequently, no reliable test results could be obtained for triaryllead hydroxides and also for some stannoxanes. This was also confirmed by others *e.g.* for triphenyltin hydroxide [66,67]. Some poorly water soluble stannoxanes were tested and showed high cytotoxicity [68–72]. Several series of organotin(IV) compounds containing diazenyl group were studied for some years and no signs of hydrolysis were observed during spectroscopic measurements and *in vitro* testing protocols. These compounds invariably displayed different ID_{50} values and different reactivities towards enzymes. The organotin(IV) compounds studied may form intermediates in test medium containing tumor cells as with many cytotoxic compounds, but there was no sign of a common intermediate.

The triphenyltin(IV) complexes of the present investigation deserve specific mention. In complexes (**4**–**7**), the triphenyltin(IV) carboxylate is *o*-positioned in the diazo-forming moiety, while in compounds **1**–**3** it is *p*-positioned (see Scheme 1). The cytotoxicity data (ID_{50}) for the test complexes (**1**–**3**) are of the same order of magnitude and the change of ligand substitution does not influence the cytotoxic activity significantly. The results of **1**–**3** are also comparable to that of its *o*-analogs, i.e. **4**–**7**, except **5**. Pair wise comparison of the

Table 5
In vitro ID_{50} values (ng/ml) of test complexes **1–5**, reported organotin(IV) complexes (**6–20**) and standard drugs using cell viability tests in seven human tumor cell lines[a].

Test complex[b]	Cell lines						
	A498	EVSA-T	H226	IGROV	M19 MEL	MCF-7	WIDR
Ph_3SnL^1H (**1**)	103	43	102	107	100	53	102
Ph_3SnL^2H (**2**)	103	41	101	107	98	43	100
Ph_3SnL^3H (**3**)	101	35	102	110	101	41	105
Ph_3SnL^4H (**4**)	101	43	102	111	103	79	106
Ph_3SnL^5H (**5**)[c] [29]	162	97	148	214	118	113	106
Ph_3SnL^6H (**6**)[d] [27]	101	41	104	109	103	92	104
Ph_3SnL^7H (**7**)[d] [27]	103	49	101	101	104	78	95
Bu_3SnL^2H (**8**)[e] [61]	182	101	163	239	125	118	106
Bu_3SnL^3H (**9**)[e] [61]	177	27	167	269	127	112	105
Bu_3SnL^4H (**10**)[e] [61]	176	100	165	253	126	120	105
Bu_3SnL^5H (**11**)[e] [61]	162	97	148	214	118	113	106
$[Ph_3SnL^3H]_n$ (**12**)[f] [26]	96	35	56	90	42	36	33
$[Ph_3SnL^4H]_n$ (**13**)[f] [26]	104	49	111	99	75	76	42
$[Ph_3SnL^5H]_n$ (**14**)[f] [26]	39	31	38	46	36	34	31
$[Ph_3SnL^6H]_n.nCCl_4$ (**15**)[f] [25]	105	81	105	101	102	111	106
$[Ph_3SnL^7H]_n$ (**16**)[f] [25]	120	100	115	105	130	115	110
$[Ph_3SnL^8H]_n$ (**17**)[f] [25]	113	96	108	106	112	110	109
Ph_3SnR_1 (**18**)[g] [23]	42	<3	39	19	42	17	17
Ph_3SnR_2 (**19**)[g] [23]	65	<3	61	18	51	16	19
Ph_3SnR_3 (**20**)[g] [23]	<2	<2	<2	<2	<2	2.9	<2
DOX	90	8	199	60	16	10	11
CDDP	2253	422	3269	169	558	699	967
5-FU	143	475	340	297	442	750	225
MTX	37	5	2287	7	23	18	<3.2
ETO	1314	317	3934	580	505	2594	150
TAX	<3.2	<3.2	<3.2	<3.2	<3.2	<3.2	<3.2

[a] Abbreviation: DOX, doxorubicin; CDDP, cisplatin; 5-FU, 5-fluorouracil; MTX, methotrexate; ETO, etoposide and TAX, paclitaxel.
[b] Standard drug reference values are cited immediately after the test complexes under identical conditions.
[c] For reported triphenyltin(IV) complex **5**, ID_{50} values (ng/ml) are now included. Refer to Scheme 1 for ligand skeleton.
[d] ID_{50} values (ng/ml) were taken from ref. 27 for the reported triphenyltin(IV) complexes (**6** and **7**) for comparison. Refer to Scheme 1 for ligand skeletons.
[e] ID_{50} values (ng/ml) were taken from ref. 61 for the reported tributyltin(IV) complexes (**8–11**) for comparison. Refer to Scheme 1 for ligand skeletons.
[f] Reported triphenyltin(IV) complexes (**12–17**) have been included for comparison; see refs. 25 and 26: LH is a carboxylate residue where L^3H, 2-{[(2*Z*)-(3-hydroxy-1-methyl-2-butenylidene)]amino}-4-methyl-pentanoate; L^4H, 2-{[(*E*)-1-(2-hydroxyphenyl)- methylidene]amino}-4-methyl-pentanoate; L^5H, 2-{[(*E*)-1-(2-hydroxyphenyl)-ethylidene]amino}-4-methyl-pentanoate; L^6H, 2-{[(2*Z*)-(3-hydroxy-1-methyl-2-butenylidene)]amino}phenylpropionate; L^7H, 2-{[(*E*)-1-(2-hydroxyphenyl)methylidene]- amino}phenylpropionate; L^8H, 2-{[(*E*)-1-(2-hydroxyphenyl)ethylidene]amino}-phenylpropionate.
[g] Reported triphenyltin(IV) complexes (**18–20**) have been included for comparison; see ref. 23: R is a carboxylate residue where R_1 = − terebate, R_2 = − steroidcarboxylate, R_3 = − benzocrowncarboxylate.

complexes, wherein the ligand nuclear substituents are held constant, was also necessary to judge the influence of the *p*- and *o*- derivatives. For pair **1** and **5**, the *p*- derivative **1** is found to be more active, while for pairs **3** and **4**, and **2** and **6**, both *p*- and *o*- derivatives displayed comparable activity. Upon closer inspection of the ID_{50} values of **1** and **5**, one can see that **1** is two folds more cytotoxic than **5** for the cell line MCF-7 and similar observations were noted for pairs **3** and **4**, and **2** and **6**. As noted, **5** is an exception; its lower cytotoxicity might be the result of internal co-ordination of OH with Sn. This can make the Sn less attractive for co-ordination with DNA or sugar moieties. The larger t-Bu group might impede the internal co-ordination. In a manner similar to **4–7**, a comparison is possible for Ph_3SnLH (**2–4**) and Bu_3SnLH (**8–11**) since each set of complexes contains a common ligand frame work. Triphenyltin(IV) complexes **2–4** were found to be more active than corresponding tributyltin(IV) complexes **8–11**. In general, the cytotoxic results of complexes **1–3** are undoubtedly far superior to CDDP, 5-FU and ETO, and related tributyltin(IV) complexes **8–11**. Triphenyltin(IV) complexes **1–3** deserve merit over their *o*-analogs (**4–6**) for better activity, particularly against MCF-7 cell line. On the other hand, although the ID_{50} values for the test complexes (**1–4**) of the present investigation are also similar to that of the triphenyltin(IV) complexes of Schiff bases derived from *L*-leucine and phenylalanine [25,26], their advantage lies in the stability. It should be mentioned here that the triphenyltin(IV) 2/4-[(*E*)-2-(aryl)-1-diazenyl]benzoates (**1–7**) are stable for a significantly longer period in both the solid-state and in solution than triphenyltin (IV) complexes containing amino acetate skeletons [25,26]. Thus, the cytotoxicity data of complexes **1–3**, together with better solubility, is suggestive of promising candidates for further *in vitro* and *in vivo* studies after appropriate modifications. The cytotoxicity data of complexes **1–3** further indicate that structural variation of the L-R skeletons does not influence the activity. However, attempts were made to provide additional precise information from the quantitative structure-activity relationship (see below).

3.4. QSAR studies

From the cytotoxicity data [log $1/ID_{50}$ (mol l^{-1})] of organotin(IV) compounds **1–11** in Table 6, the following QSAR models 1–7 were developed:QSAR for the cytotoxicity of compounds **1–11** against A498 human tumor cell line (Table 6)

$$\log 1/ID_{50(A498)} = -0.07(\pm 0.05)\,\text{Clog P} + 0.10(\pm 0.04)\text{CMR} + 5.47(\pm 0.81)$$
$$n = 11, r^2 = 0.826, s = 0.065, q^2 = 0.738, Q = 13.985, F_{2,8} = 18.989(4.459) \quad (1)$$

QSAR for the cytotoxicity of compounds **1–11** against EVSA-T human tumor cell line (Table 6)

$$\log 1/ID_{50(EVSA-T)} = -0.11(\pm 0.05)\,\text{Clog P} + 0.17(\pm 0.04)\text{CMR} + 5.15(\pm 0.68)$$
$$n = 9, r^2 = 0.959, s = 0.051, q^2 = 0.899, Q = 19.196, F_{2,6} = 70.171(5.143) \quad (2)$$

outliers: compounds **5** and **9**

QSAR for the cytotoxicity of compounds **1–11** against H226 human tumor cell line (Table 6)

$$\log 1/ID_{50(H226)} = -0.06(\pm 0.04)\,\text{Clog P} + 0.09(\pm 0.04)\text{CMR} + 5.70(\pm 0.67)$$
$$n = 11, r^2 = 0.841, s = 0.053, q^2 = 0.755, Q = 17.302, F_{2,8} = 21.157(4.459) \quad (3)$$

QSAR for the cytotoxicity of compounds **1–11** against IGROV human tumor cell line (Table 6)

$$\log 1/ID_{50(IGROV)} = -0.12(\pm 0.08)\,\text{Clog P} + 0.14(\pm 0.07)\text{CMR} + 5.22(\pm 1.23)$$
$$n = 11, r^2 = 0.807, s = 0.098, q^2 = 0.707, Q = 9.163, F_{2,8} = 16.725(4.459) \quad (4)$$

QSAR for the cytotoxicity of compounds **1–11** against M19 MEL human tumor cell line (Table 6)

$$\log 1/ID_{50(M19MEL)} = -0.03(\pm 0.02)\,\text{Clog P} + 0.05(\pm 0.02)\text{CMR} + 6.13(\pm 0.30)$$
$$n = 11, r^2 = 0.887, s = 0.024, q^2 = 0.823, Q = 39.25, F_{2,8} = 31.398(4.459) \quad (5)$$

QSAR for the cytotoxicity of compounds **1–11** against MCF-7 human tumor cell line (Table 6)

$$\log 1/ID_{50(MCF-7)} = -0.14(\pm 0.05)\,\text{Clog P} + 0.18(\pm 0.04)\text{CMR} + 5.10(\pm 0.69)$$
$$n = 7, r^2 = 0.983, s = 0.039, q^2 = 0.947, Q = 25.410, F_{2,4} = 115.647(6.944) \quad (6)$$

outliers: compounds **4–7**

Table 6
Comparison between observed and predicted log $1/ID_{50}$ (mol l^{-1}), Clog P, and CMR of **1–11.**

No.	Compound	log $1/ID_{50}$ (A498) (Eq. (1))		log $1/ID_{50}$ (EVSA-T) (Eq. (2))		log $1/ID_{50}$ (H226) (Eq. (3))		log $1/ID_{50}$ (IGROV) (Eq. (4))	
		Obsd.	Pred.	Obsd.	Pred.	Obsd.	Pred.	Obsd.	Pred.
1	Ph_3SnL^1H	6.77	6.73	7.15	7.13	6.77	6.74	6.75	6.70
2	Ph_3SnL^2H	6.77	6.74	7.17	7.14	6.78	6.75	6.75	6.71
3	Ph_3SnL^3H	6.81	6.79	7.27	7.21	6.80	6.78	6.77	6.73
4	Ph_3SnL^4H	6.81	6.79	7.18	7.21	6.80	6.78	6.77	6.73
5[a]	Ph_3SnL^5H	6.57	6.73	6.80	7.13	6.61	6.74	6.45	6.70
6	Ph_3SnL^6H	6.78	6.74	7.17	7.14	6.76	6.75	6.74	6.71
7	Ph_3SnL^7H	6.78	6.77	7.10	7.19	6.79	6.77	6.79	6.75
8	Bu_3SnL^2H	6.48	6.49	6.73	6.73	6.52	6.53	6.36	6.35
9[a]	Bu_3SnL^3H	6.52	6.54	7.34	6.81	6.55	6.57	6.34	6.38
10	Bu_3SnL^4H	6.52	6.54	6.77	6.81	6.55	6.57	6.37	6.38
11	Bu_3SnL^5H	6.53	6.48	6.75	6.73	6.57	6.53	6.41	6.35

No.	Compound	log $1/ID_{50}$ (M19 MEL) (Eq. (5))		log $1/ID_{50}$ (MCF-7) (Eq. (6))		log $1/ID_{50}$ (WIDR) (Eq. (7))		Clog P	CMR
		Obsd.	Pred.	Obsd.	Pred.	Obsd.	Pred.		
1	Ph_3SnL^1H	6.78	6.76	7.06	7.11	6.77	6.76	6.79	16.63
2	Ph_3SnL^2H	6.79	6.77	7.15	7.12	6.78	6.76	6.74	16.63
3	Ph_3SnL^3H	6.81	6.80	7.20	7.17	6.79	6.80	8.11	18.02
4[b]	Ph_3SnL^4H	6.80	6.80	6.91	7.17	6.79	6.80	8.11	18.02
5[b]	Ph_3SnL^5H	6.71	6.76	6.73	7.11	6.76	6.76	6.79	16.63
6[b]	Ph_3SnL^6H	6.77	6.77	6.82	7.12	6.76	6.76	6.74	16.63
7[b,c]	Ph_3SnL^7H	6.77	6.78	6.90	7.18	6.81	6.76	6.37	16.67
8	Bu_3SnL^2H	6.64	6.65	6.66	6.66	6.71	6.72	7.44	14.66
9	Bu_3SnL^3H	6.67	6.67	6.72	6.72	6.75	6.75	8.81	16.06
10	Bu_3SnL^4H	6.67	6.67	6.69	6.72	6.75	6.75	8.81	16.06
11	Bu_3SnL^5H	6.66	6.64	6.68	6.66	6.71	6.72	7.49	14.66

[a] Not included in the derivation of QSAR 2.
[b] Not included in the derivation of QSAR 6.
[c] Not included in the derivation of QSAR 7.

QSAR for the cytotoxicity of compounds **1–11** against WIDR human tumor cell line (Table 6)

$$\log 1/ID_{50(WIDR)} = 0.024(\pm 0.006)\,CMR + 6.371(\pm 0.104)$$
$$n = 10, r^2 = 0.903, s = 0.009, q^2 = 0.856, Q = 105.556, F_{1,8} = 74.474 (5.318) \quad (7)$$

outlier: compound **7**

QSAR models 1–6 are well defined by two descriptors; Clog P and CMR (Fig. 4 of QSAR 5 represents the best example). But for the QSAR 7, the cytotoxic activity is well correlated with only the CMR term and there is no role of hydrophobic parameter. On comparing the statistical contribution of Clog P and CMR descriptors, it has been found that CMR is a more important parameter than that of Clog P. CMR explains 65%, 77%, 63%, 54%, 72%, 72%, and 90%, respectively, of the variance in the data of QSAR models 1–7, while Clog P accounts for only 18%, 19%, 21%, 27%, 17%, and 27%, respectively, of the variance in the data of QSAR models 1–6. Thus CMR (steric/polarizability factor) plays a major role for the cytotoxicity of organotin(IV) compounds **1–11** against a panel of seven human tumor cell lines studied.

Compounds were deemed to be outliers in QSARs (Eqs. (2), (6), and (7)) on the basis of deviations in their activities (obsd – pred $> 2 \times s$). To assess the effects of excluding outlier(s), QSAR models were examined thoroughly before and after the removal of a compound. Although QSAR 6 is a very good model with respect to their statistics, we could not consider it as a predictive model. This is because the QSAR 6 was developed for a very small data set using two descriptors and also after removing four outliers. A large number of outliers for this QSAR model may suggest the combination of used descriptors (Clog P and CMR) is not sufficient enough and may need the additional descriptor(s), but the additional descriptor(s) cannot be considered due to the very small data set. Lastly, we kept this equation only for the comparison point of view.

The presence of Clog P term with negative coefficient in QSARs 1–6 suggests that the cytotoxicity of compounds **1–11** decreases with increasing hydrophobicity against six cancer cell lines (*e.g.* A498, EVSA-T, H226, IGROV, M19 MEL, and MCF-7). On the contrary, the cytotoxicity of these compounds increases with increasing their steric/polarizability (CMR) against all the seven cancer cell lines as evident by the positive coefficient of the CMR term. Although there are high statistics associated with QSARs 1–6 ($r^2 = 0.807$–0.983), the C log P of compounds **1–11** with high values (6.37–8.81) are not great enough to establish the upper limit of the activity, these compounds may have higher C log P values than that of the optimum. It suggests that QSARs 1–6 may represent only the second half of the parabolic/bilinear model in terms of C log P, which may be the cause for the presence of negative C log P term in QSARs 1–6. Thus, more compounds with lower C log P (C log P<6.37) values will be needed to establish the upper C log P limit either for the development of a parabolic or bilinear QSAR model.

On comparison among QSAR models 1–7, one can suggest that the mechanism for the cytotoxic activity of compounds **1–11** against A498, EVSA-T, H226, IGROV, M19 MEL, and MCF-7 cancer cell lines is almost the same and depends directly on the hydrophobic and molar refractivity parameters of the compound. It must be noted here that QSARs 1 and 3–5 explain 82.3–88.2% of the variance in the data sets without any outlier, but QSARs 2 and 6 explain 95.9% and 98.3% of the variance in the data sets with the help of 2 and 4 outliers, respectively. Thus QSARs 2 and 6 are not exactly the same to that of QSARs 1 and 3–5. Now, it can be concluded that the mechanism for the cytotoxic activity of compounds **1–11** against A498, H226, IGROV, and M19 MEL cancer cell lines is almost the same, but somewhat different from that of against EVSA-T and MCF-7 cancer cell lines. These cancer cell lines may have some different mechanism in addition to the common one. On the other hand, QSAR 7 explains 90.3% of the variance in the data set using only one CMR descriptor and one outlier. There is no room to accommodate the hydrophobic term in this QSAR model, which suggests that the cytotoxic activity of compounds **1–11** against WIDR cancer cell line may have some different mechanism in comparison to that of the other six cancer cell lines such as A498, EVSA-T, H226, IGROV, M19 MEL, and MCF-7. The similar mechanism for the cytotoxic activity of compounds **1–11** against A498, H226, IGROV, and M19 MEL cancer cell lines can also be demonstrated by very high mutual correlations ($r^2 = 0.948$–0.996) in activity–activity relationships i.e. the direct comparison among the cytotoxic activity of compounds **1–11** against A498, H226, IGROV, and M19 MEL cancer cell lines as shown in Table 7 and Figs. 5, S4–S8.

3.4.1. Validation of QSAR models

Two steps, statistical diagnostics and internal validation, were used to validate QSAR models 1–7. In statistical diagnostics, QSARs 1–7 were filtered through the following conditions: (i) $n/p \geq 4$ (except QSAR 6) (ii) $r^2 > 0.6$ (iii) $q^2 > 0.5$ (iv) $r^2 - q^2 < 0.3$ (v) $F > F_{(lit)}$ at 95% level (vi) high Q value, and (vii) low s value [43,73-78]. On the other hand, the internal validation was carried out by using cross-validation ($q^2 > 0.5$) [74,77]. Since there is not sufficient difference in activities of compounds, there is probability of a chance correlation in the QSAR models. To examine this problem, we performed a Y-randomization test. According to this test, if a strong correlation remains between the selected descriptor(s) and the randomly permuted response, the significance of the proposed QSAR is suspect [44,73,77,78]. In the Y-randomization test, the poor values of r^2 and q^2 in Table 8 ensure the robustness of the QSAR models 1–7 and also the lack of over fitting. Due to the small data sets, the external

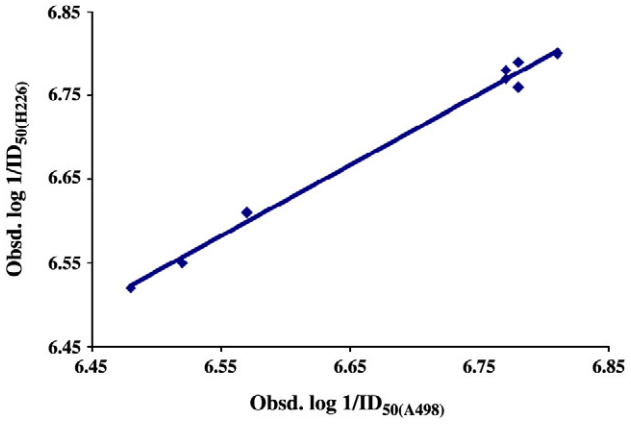

Fig. 5. Plot of observed log $1/ID_{50(A498)}$ versus observed log $1/ID_{50(H226)}$ (Table 7).

Table 7
Statistical data for the correlations among the cytotoxic activities of compounds **1**–**11** (n = 11) against four cancer cell lines *e.g.* A498, H226, IGROV, and M19 MEL.

Correlations	r^2	q^2	s	Slope
log $1/ID_{50(A498)}$ *vs* log $1/ID_{50(H226)}$	0.996	0.994	0.010	−1.04 (±0.39)
log $1/ID_{50(A498)}$ *vs* log $1/ID_{50(IGROV)}$	0.983	0.972	0.019	2.14 (±0.46)
log $1/ID_{50(A498)}$ *vs* log $1/ID_{50(M19\ MEL)}$	0.976	0.968	0.023	−7.69 (±1.70)
log $1/ID_{50(H226)}$ *vs* log $1/ID_{50(IGROV)}$	0.990	0.984	0.013	2.75 (±0.30)
log $1/ID_{50(H226)}$ *vs* log $1/ID_{50(M19\ MEL)}$	0.981	0.972	0.018	−5.76 (±1.32)
log $1/ID_{50(IGROV)}$ *vs* log $1/ID_{50(M19\ MEL)}$	0.948	0.924	0.048	−13.83 (±3.59)

validation test was not considered. Although QSAR models 1–7 have been passed through all the necessary validation tests, we did not consider these models as the predictive QSAR models due to the presence of low activity range (<1 log unit) in the data sets. To construct the predictive QSAR models, we need to synthesize additional organotin(IV) compounds similar to compounds **1**–**11** with lower C log P (C log P<6.37) and higher/similar CMR values. It is interesting to note that there is no mutual correlation between C log P and CMR of compounds **1**–**11** (C log P *vs* CMR; $r = 0.025$), providing us enough space to manipulate the structure of organotin(IV) compounds **1**–**11** with respect to their varying C log P and CMR in order to obtain the compound with desired activity.

4. Conclusions and outlook

We reported here the syntheses, characterization and cytotoxic activities of some new triphenyltin(IV) 2/4-[(*E*)-2-(aryl)-1-diazenyl] benzoates (**1**–**4**). Our studies have demonstrated the potential of developing compounds **1**–**4** as effective cytotoxic agents on all the cell lines studied, particularly MCF-7 with an ID_{50} range of 41–53 ng/ml in vitro. Complexes **1**–**4** appear to display similar cytotoxicity, irrespective of their nuclear substituents in the coupling moiety. From QSAR models 1–7 it can be suggested that the cytotoxicity of compounds **1**–**11** against the four different cancer cell lines (A498, H226, IGROV, and M19 MEL) are due to a very similar mechanism, but the same is not true against the EVSA-T, MCF-7, and WIDR cancer cell lines. These three cancer cell lines may have some different mechanism in addition to the common one. The triphenyltin(IV) 2/4-[(*E*)-2-(aryl)-1-diazenyl]benzoates (**1**–**4**) may therefore be explored further by *in vivo* testing in animal models to develop them as anticancer chemotherapeutics. Further work in this area is underway.

Acknowledgments

The financial support of the Department of Science and Technology, New Delhi, India (Grant No. SR/S1/IC-03/2005,TSBB), the council of Scientific and Industrial Research, New Delhi, India (Grant No. 09/347/(0197)/2011/EMR I, for an award of a Senior Research Fellowship, AP), of the Università degli Studi di Palermo, Italy (Grants ORPA079E5M and ORPA0737W2) and the University Grants Commission, New Delhi, India through SAP-DSA, Phase-III, are gratefully acknowledged. The *in vitro* cytotoxicity experiments were carried out by Ms. P. F. van Cuijk in the Laboratory of Translational Pharmacology, Department of Medical Oncology, Erasmus Medical Center, Rotterdam, The Netherlands, under the supervision of Dr. E. A. C. Wiemer and Prof. Dr. G. Stoter.

Appendix A. Supplementary material

Crystallographic data for complexes **1**, **3** and **4** reported in this paper have been deposited with the Cambridge Crystallographic Data Centre (CCDC) as supplementary publication no. CCDC-822371–CCDC-822373. Copies of the data can be obtained free of charge from the CCDC (12 Union Road, Cambridge CB2 1EZ, UK; Tel.: +44-1223-336408; Fax: +44-1223-336003; e-mail: deposit@ccdc.cam.ac.uk; Web site: http://www.ccdc.cam.ac.uk).

The following information (Figs. S1–S8) are available as supplementary materials. Fig S1: Diagram (PLATON) of a unit cell in compound **1**. The short intramolecular hydrogen bonds have been drawn as dashed lines. H atoms bonded to C have been omitted; Fig. S2: Diagram (PLATON) of a unit cell in compound **3**. The short intramolecular hydrogen bonds have been drawn as dashed lines. H atoms bonded to C have been omitted; Fig. S3: Diagram (PLATON) of a unit cell in compound **4**. The short intramolecular hydrogen bonds have been drawn as dashed lines. H atoms bonded to C have been omitted; Fig. S4: Plot of observed log 1/ID50(A498) versus observed log 1/ID50(IGROV) (Table 7); Fig. S5: Plot of observed log 1/ID50(A498) versus observed log 1/ID50(M19 MEL) (Table 7); Fig. S6: Plot of observed log 1/ID50(H226) versus observed log 1/ID50(IGROV) (Table 7); Fig. S7: Plot of observed log 1/ID50(H226) versus observed log 1/ID50(M19 MEL) (Table 7); Fig. S8: Plot of observed log 1/ID50(IGROV) versus observed log 1/ID50(M19 MEL) (Table 7).

Supplementary data to this article can be found online at doi:10.1016/j.jinorgbio.2011.10.008.

Table 8
Y-randomization test data for QSARs 1–7.

QSAR no.	NOR-1[a]		NOR-2		NOR-3		NOR-4		NOR-5	
	r^2	q^2	r^2	q^2	r^2	q^2	r^2	q^2	r^2	q^2
1	0.320	−0.216	0.247	−0.314	0.562	0.270	0.342	−0.183	0.244	−0.328
2	0.271	−0.452	0.203	−0.478	0.648	0.203	0.390	−0.180	0.115	−1.370
3	0.366	−0.113	0.265	−0.311	0.591	0.315	0.373	−0.155	0.266	−0.288
4	0.385	−0.064	0.310	−0.220	0.576	0.306	0.405	−0.114	0.328	−0.180
5	0.372	−0.089	0.205	−0.423	0.642	0.406	0.378	−0.115	0.221	−0.342
6	0.391	−0.347	0.232	−0.944	0.694	−0.405	0.648	−0.147	0.245	−0.886
7	0.242	−0.224	0.028	−0.407	0.311	0.006	0.052	−0.438	0.197	−0.151

[a] NOR = number of Y-randomization.

References

[1] V.L. Narayanan, M. Nasr, K.D. Paul, in: M. Gielen (Ed.), Tin-based Antitumour Drugs, Springer-Verlag, Berlin, 1990, pp. 201–217.
[2] A.J. Crowe, Metal Based Antitumour Drugs, in: M. Gielen (Ed.), vol. 1, Freund, London, 1988, pp. 103–149.
[3] M. Gielen, P. Lelieveld, D. de Vos, R. Willem, in: M. Gielen (Ed.), vol. 2, Freund, Tel Aviv, 1992, pp 29–54.
[4] C. Pellerito, P. D'Agati, T. Fiore, C. Mansueto, V. Mansueto, G. Stocco, L. Nagy, L. Pellerito, J. Inorg. Biochem. 99 (2005) 1294–1305.
[5] F. Cima, L. Ballarin, Appl. Organomet. Chem. 13 (1999) 697–703.
[6] M.N. Shuaibu, H. Kanbara, T. Yanagi, A. Ichinose, D.A. Ameh, J.J. Bonire, A.J. Nok, Jpn. Parasitol. Res. 91 (2003) 5–11.
[7] C.-R. Jan, B.-P. Jiann, Y.-C. Lu, H.-T. Chang, W. Su, W.-C. Chen, C.-C. Yu, J.-K. Huang, Life Sci. 70 (2002) 1337–1345.
[8] M.P. Samuel, D. de Vos, D. Raveendra, J.A.R.P. Sarma, S. Roy, Bioorg. Med. Chem. Lett. 12 (2002) 61–64.
[9] C.E. Carraher Jr., A. Battin, K.R. Shahi, M.R. Roner, J. Inorg. Organomet. Polym. 17 (2007) 631–639.
[10] G. Barot, K.R. Shahi, M.R. Roner, C.E. Carraher Jr., J. Inorg. Organomet. Polym. 17 (2007) 595–603.
[11] M. Roner, C. Carraher, T. Sabir, K. Shahi, J. Roehr, K. Bassett, Polym. Mater. Sci. Eng. 95 (2006) 525–527.
[12] C. Carraher, Y. Ashida, G. Battin, Polym. Mater. Sci. Eng. 95 (2006) 556–558.
[13] C. Carraher, T. Sabir, M. Roner, K. Shahi, R. Bleicher, J. Roehr, K. Bassett, J. Inorg. Organomet. Polym. 16 (2006) 249–257.
[14] M. Roner, C. Carraher, J. Roehr, K. Bassett, J. Polym. Mater. 23 (2006) 153–159.
[15] C. Carraher, D. Siegmann-Louda, Macromolecules containing metal and metal-like elements, Biomedical Applications, vol. 3, Wiley, Hoboken, NJ, 2004.
[16] R. Doucette, D. Siegmann-Louda, C. Carraher, A. Cardoso, Polym. Mater. Sci. Eng. 91 (2004) 564–566.
[17] P.J. Blower, Annu. Rep. Prog. Chem. A 100 (2004) 633–658.
[18] M. Gielen, R. Willem, M. Biesemans, M. Boučlam, A. El Khloufi, D. de Vos, Appl. Organomet. Chem. 6 (1992) 287–291.
[19] M. Kemmer, M. Gielen, M. Biesemans, D. de Vos, R. Willem, Metal-Based Drugs 5 (1998) 189–196.
[20] M. Kemmer, L. Ghys, M. Gielen, M. Biesemans, E.R.T. Tiekink, R. Willem, J. Organomet. Chem. 582 (1999) 195–203.
[21] M. Gielen, P. Lelieveld, D. de Vos, H. Pan, R. Willem, M. Biesemans, H.H. Fiebig, Inorg. Chim. Acta 196 (1992) 115–117.
[22] M. Boučlam, M. Gielen, A. El Khloufi, D. de Vos, R. Willem, Eur. Pat., Publ. 538 517, Appl 91/202, 746.3-, 22.10.91; Chem. Abstr. 119 (1993) 117548b.
[23] M. Gielen, E.R.T. Tiekink (Eds.), Metallotherapeutic Drug and Metal-based Diagnostic Agents: ^{50}Sn Tin Compounds and their Therapeutic Potential, Wiley, Chichester, England, 2005, pp. 421–439, (and references therein).
[24] M. Gielen, R. Willem, H. Dalil, D. de Vos, C.M. Kuiper, G.J. Peters, Metal-Based Drugs 5 (1998) 83–90.
[25] T.S. Basu Baul, C. Masharing, G. Ruisi, R. Jirásko, M. Holčapek, D. de Vos, D. Wolstenholme, A. Linden, J. Organomet. Chem. 692 (2007) 4849–4862.
[26] T.S. Basu Baul, S. Basu, D. de Vos, A. Linden, Invest. New Drugs 27 (2009) 419–431.
[27] T.S. Basu Baul, A. Paul, L. Pellerito, M. Scopelliti, P. Singh, P. Verma, D. de Vos, Invest. New Drugs 28 (2010) 587–599.
[28] P. Singh, A. Bhardwaj, Mini Rev. Med. Chem. 8 (2008) 388–398.
[29] R. Willem, I. Verbruggen, M. Gielen, M. Bieseman, B. Mahieu, T.S. Basu Baul, E.R.T. Tiekink, Organometallics 17 (1998) 5758–5766.
[30] B. Kushlefsky, I. Simmons, A. Ross, Inorg. Chem. 2 (1963) 187–189.
[31] T.S. Basu Baul, A. Paul, L. Pellerito, M. Scopelliti, P. Singh, P. Verma, A. Duthie, D. de Vos, E.R.T. Tiekink, Invest. New Drugs 29 (2011) 285–299.
[32] T.S. Basu Baul, A. Paul, E.R.T. Tiekink, Acta Crystallogr. E66 (2010) o540.
[33] T.S. Basu Baul, A. Paul, H.D. Arman, E.R.T. Tiekink, Acta Crystallogr. E64 (2008) o2125.
[34] M.R. Boyd, Status of the NCI preclinical antitumor drug discovery screen, in: V.T. DeVita Jr., S. Hellman, S.A. Rosenberg (Eds.), Cancer: Principles and Practice of Oncology Updates, vol. 3, J.P. Lippincott, Philadelphia, 1989, pp. 1–12.
[35] Y.P. Keepers, P.R. Pizao, G.J. Peters, J.V. Ark-Otte, B. Winograd, H.M. Pinedo, Eur. J. Cancer 27 (1991) 897–900.
[36] C-QSAR Program, BioByte Corp., 201 W. 4th St., Suite 204, Claremont, CA 91711, USA, www.biobyte.com.
[37] C. Hansch, D. Hoekman, A. Leo, D. Weininger, C.D. Selassie, Chem. Rev. 102 (2002) 783–812.
[38] R.P. Verma, C. Hansch, Development of QSAR models using C-QSAR program: a regression program that has dual database of over 21,000 QSAR models freely available at: Nat. Protoc. (2007) (Nature Publishing Group), Freely available at: http://www.nature.com/protocolexchange/protocols/181, doi:10.1038/nprot.2007.125.
[39] R.P. Verma, C. Hansch, Chem. Rev. 109 (2009) 213–235.
[40] R.P. Verma, C. Hansch, Chem. Rev. 111 (2011) 2865–2899.
[41] C. Selassie, R.P. Verma, History of quantitative structure-activity relationships, in: D.J. Abraham, D.P. Rotella (Eds.), Burger's Medicinal Chemistry, 7th edition, Drug Discovery and Development, vol. 1, John Wiley, New York, USA, 2010, pp. 1–95, 2010.
[42] R.D. Cramer III, J.D. Bunce, D.E. Patterson, I.E. Frank, Quant. Struct.-Act. Relat. 7 (1988) 18–25.
[43] C.A. Bennett, N.L. Franklin, Statistical Analysis in Chemistry and the Chemical Industry, John Wiley, New York, 1967, pp. 708–709.
[44] C.D. Selassie, S. Kapur, R.P. Verma, M. Rosario, J. Med. Chem. 48 (2005) 7234–7242.
[45] SAINT + V. 6.45, Program for Reduction of Data Collected on Bruker CCD Area Detector Diffractometer, Bruker, Madison, Wisconsin, USA, 2003.
[46] SADABS V. 2004/1, Program for the Absorption of Area Detector Data, Bruker, Madison, Wisconsin, USA, 2004.
[47] G.M. Sheldrick, Acta Crystallogr. A64 (2008) 112–122.
[48] T.S. Basu Baul, S.M. Pyke, K.K. Sarma, E.R.T. Tiekink, Main Group Met. Chem. 19 (1996) 807–814.
[49] J. Holeček, M. Nádvorník, K. Handlíř, A. Lyčka, J. Organomet. Chem. 241 (1983) 177–184.
[50] T.S. Basu Baul, S. Dhar, S.M. Pyke, E.R.T. Tiekink, E. Rivarola, R. Butcher, F.E. Smith, J. Organomet. Chem. 633 (2001) 7–17.
[51] G.M. Bancroft, R.H. Platt, Adv. Inorg. Chem. Rad. 15 (1972) 59–258.
[52] R.L. Collins, J.C. Travis, in: I.J. Gruverman (Ed.), The Electric Field Gradient Tensor: Mössbauer Effect Methodology, vol. 3, Plenum Press, New York, 1967, pp. 123–161.
[53] G.M. Bancroft, V.G. Kumar Das, T.K. Sham, M.G. Clark, J. Chem. Soc. Dalton Trans. (1976) 643–654.
[54] T.K. Sham, G.M. Bancroft, Inorg. Chem. 14 (1975) 2281–2283.
[55] M.G. Clark, A.G. Maddock, R.H. Platt, J. Chem. Soc. Dalton Trans. (1972) 281–290.
[56] R.V. Parish, in: G.J. Long (Ed.), Structure and Bonding in Tin Compound: Mössbauer Spectroscopy Applied to Inorganic Chemistry, vol. 1, Plenum Press, New York, 1984, pp. 544–548.
[57] P.J. Harrison, K. Lambert, T.J. King, B. Majee, J. Chem. Soc. Dalton Trans. (1983) 363–369.
[58] T.S. Basu Baul, E.R.T. Tiekink, Z. Kristallogr. (NCS) 211 (1996) 489–490.
[59] T.S. Basu Baul, S. Dhar, N. Kharbani, S.M. Pyke, R. Butcher, F.E. Smith, Main Group Met. Chem. 22 (1999) 413–421.
[60] T.S. Basu Baul, W. Rynjah, E. Rivarola, A. Linden, J. Organomet. Chem. 690 (2005) 613–621.
[61] T.S. Basu Baul, A. Paul, L. Pellerito, M. Scopelliti, C. Pellerito, P. Singh, P. Verma, A. Duthie, D. de Vos, R.P. Verma, U. Englert, J. Inorg. Biochem. 104 (2010) 950–966.
[62] M.C. Etter, J.C. MacDonald, J. Bernstein, Acta Crystallogr. B46 (1990) 256–262.
[63] C.J. Tranter, S.B. Price, J. Cutts, P.G. Parsons, G. Rintoul, D.J. Young, Main Group Chem. 1 (1995) 165–167.
[64] S.C. Ng, P.G. Parsons, K.Y. Sim, C.J. Tranter, R.H. White, Appl. Organometal. Chem. 11 (1997) 577–578.
[65] M. Gielen, E.R.T. Tiekink, Tin compounds and their therapeutic potential, in: M. Gielen, E.R.T. Tiekink (Eds.), Metallotherapeutic Drugs and Metal-Based Diagnostic Agents: The Use of Metals in Medicine, John Wiley & Sons, London, 2005, pp. 421–439.
[66] R.A. LeBoeuf, G.A. Kerkaert, M.J. Aardema, D.P. Gibson, R. Brauninger, R.J. Isfort, Mut. Res. 356 (1996) 85–127.
[67] R.J. Isfort, G.A. Kerckaert, R.A. LeBoeuf, Mut. Res. 356 (1996) 11–63.
[68] A. Meriem, R. Willem, M. Biesemans, B. Mahieu, D. de Vos, P. Lelieveld, M. Gielen, Appl. Organometal. Chem. 5 (1991) 195–201.
[69] M. Gielen, P. Lelieveld, D. de Vos, R. Willem, Metal-Based Anti-Tumour Drugs 2 (1992) 29–54.
[70] H. Dalil, M. Biesemans, R. Willem, M. Gielen, Main Group Met. Chem. 21 (1998) 741–745.
[71] S.W. Ng, J.M. Hook, M. Gielen, Appl. Organometal. Chem. 14 (2000) 1–7.
[72] C. Camacho-Camacho, D. de Vos, B. Mahieu, M. Gielen, M. Kemmer, M. Biesemans, R. Willem, Main Group Met. Chem. 23 (2000) 433–438.
[73] C. Hansch, R.P. Verma, ChemMedChem 2 (2007) 1807–1813.
[74] A. Golbraikh, A. Tropsha, J. Mol. Graph Modl. 20 (2002) 269–276.
[75] L. Eriksson, J. Jaworska, A.P. Worth, M.T.D. Cronin, R.M. McDowell, P. Gramatica, Environ. Health Prospect. 111 (2003) 1361–1375.
[76] L. Pogliani, Chem. Rev. 100 (2000) 3827–3858.
[77] A. Tropsha, P. Gramatica, V.K. Gombar, QSAR Comb. Sci. 22 (2003) 69–77.
[78] S. Wold, L. Eriksson, Statistical validation of QSAR results, in: H. van de Waterbeemd (Ed.), Validation Tools, Chemometrics Methods in Molecular Design, Methods and Principles in Medicinal Chemistry, vol. 2, VCH, Weinheim, Germany, 1995, pp. 309–318.